

# THE ECLIPSING SUPERSOFT X-RAY BINARY CAL 87

J.B. Hutchings<sup>1</sup>, D. Crampton<sup>1</sup>

Dominion Astrophysical Observatory

Herzberg Institute of Astrophysics, National Research Council of Canada

5071 W. Saanich Rd., Victoria, B.C. V8X 4M6, Canada

A.P. Cowley<sup>1</sup>, & P.C. Schmidtke<sup>1</sup>

Physics & Astronomy Dept., Arizona State University, Tempe, AZ, 85287-1504

## ABSTRACT

We present and discuss 25 spectra obtained in November 1996, covering all phases of the CAL 87 binary system. These spectra are superior both in signal-to-noise and wavelength coverage to previously published data so that additional spectral features can be measured. Photometry obtained on the same nights is used to confirm the ephemeris and to compare with light curves from previous years. Analysis of the color variation through the orbital cycle has been carried out using archival MACHO data.<sup>2</sup> When a barely resolved red field star is accounted for, there is no  $(V - R)$ -color variation, even through eclipse. There have been substantial changes in the depth of minimum light since 1988; it has decreased more than 0.5 mag in the last several years. The spectral features and radial velocities are also found to vary not only through the 0.44-day orbit but also over timescales of a year or more. Possible interpretations of these long-term changes are discussed. The 1996 spectra contain phase-modulated Balmer absorption lines not previously seen, apparently arising in gas flowing from the region of the compact star. The changes in emission-line strengths with orbital phase indicate there are azimuthal variations in the accretion disk structures. Radial velocities of several lines give different amplitudes and

---

<sup>1</sup>Visiting Astronomers, Cerro Tololo Inter-American Observatory, National Optical Astronomy Observatories, which is operated by the Association of Universities for Research in Astronomy, Inc., under contract with the National Science Foundation.

<sup>2</sup>This paper utilizes public domain data obtained by the MACHO Project, jointly funded by the US Department of Energy through Lawrence Livermore National Laboratory under contract W7405-Eng-48, the National Science Foundation through the Center for Particle Astrophysics of the University of California undercooperative agreement AST-8809616, and the Mount Stromlo and Sidings Springs Observatory by the Bilateral Science Technology and Regional Development.

phasing, making determination of the stellar masses difficult. All solutions for the stellar masses indicate that the companion star is considerably less massive than the degenerate star. The Balmer absorption-line velocities correspond to masses of  $\sim 1.4M_{\odot}$  for the degenerate star and  $\sim 0.4M_{\odot}$  for the mass donor. However, the strong He II emission lines indicate a much more massive accreting star, with  $M_X > 4M_{\odot}$ .

*Subject headings:* accretion disks – stars: binaries – stars: individual (CAL 87)  
– X-rays: stars

## 1. Introduction

CAL 87 has long been known as one of only a small number of luminous X-ray binaries in the Large Magellanic Cloud (Long, Helfand, & Grabelsky 1981, Pakull et al. 1988). Its optical spectrum, with He II and H emission lines on a very blue continuum, shows it to be similar to galactic low-mass X-ray binaries. However, its X-ray spectrum reveals CAL 87 to be one of the rare, very luminous ( $L_{bol} \geq 10^{38}$  erg s $^{-1}$ ) supersoft sources (SSS) which have little or no radiation above  $\sim 0.5$  keV (e.g. Trümper et al. 1991, Greiner 1996). The SSS are widely thought to be binaries in which a white dwarf is undergoing rapid accretion from a more massive companion, leading to steady nuclear burning on the surface of the white dwarf (van den Heuvel et al. 1992).

CAL 87 is unique among supersoft sources in having both optical and X-ray eclipses (Callanan et al. 1989, Cowley et al. 1990: CSCH) which provide extra information about the disk structure and in principle help to constrain the stellar masses. In the original spectroscopic data of CSCH, He II 4686Å emission was shown to move with  $K=40$  km s $^{-1}$  and proper phasing with respect to the eclipse so that it was interpreted as due to orbital motion of the compact star. CSCH concluded that the compact star had a mass  $\geq 6M_{\odot}$ , and hence these data implied the presence of a black hole.

However, optical spectra taken a few years later, combined with velocities from lines in the far UV (Hutchings et al. 1995), showed a quite different behavior. The velocity amplitude was larger and the phasing was very different, indicating that at times the velocities are not entirely due to orbital motion and the line-formation regions change. One problem is that spectroscopic determination of the masses is not entirely straightforward since the nearly edge-on view of the system ( $i \sim 78^{\circ}$ ) causes complications in the line profiles due to motions in the accretion disk.

In this paper we report on a series of spectroscopic data with improved signal-to-noise (S/N) and new, concurrent photometry which we obtained at CTIO in 1996 in order to conduct a more thorough investigation of CAL 87.

## 2. Observations and Data

### 2.1. Spectroscopy

CAL 87 was observed extensively during a five-night run in 1996 November with the CTIO 4-m telescope using the KPGL1 grating and Loral 3K detector. The wavelength range covered was  $\sim 3700\text{--}6700\text{\AA}$ , with resolution  $\sim 3\text{\AA}$ . Exposure times were 20 minutes, and the mean S/N was about 20 per resolution element. The one-dimensional wavelength-calibrated spectra were extracted and processed following standard IRAF procedures. Twenty-five spectra were obtained, evenly distributed through the orbital phases, with significantly better S/N and wavelength coverage than those used in the CSCH paper. Table 1 gives the journal of observations.

Figure 1 shows the spectrum of CAL 87 in and out of eclipse, with principal features identified. The spectrum is similar to other supersoft X-ray binaries, with the strongest features being emission lines of He II and hydrogen. However, the overall emission-line equivalent widths are below typical values (see Cowley et al. (1998) for comparison with other supersoft systems). The He II Pickering-series emissions are sufficiently strong that they must significantly contaminate the H Balmer emission lines. Thus, throughout this paper “H $\alpha$ ”, “H $\beta$ ”, etc. refer to the blend of hydrogen and He II Pickering lines. Also present are emission lines of the high excitation ions O VI (3811, 3834, 5290 $\text{\AA}$ , also seen in all other supersoft binaries), N V (4603, 4619 $\text{\AA}$ ), and the C III/N III blend ( $\sim 4630\text{--}50\text{\AA}$ ). There is a broad emission at 4417 $\text{\AA}$  that we have been unable to identify. It is similar in strength to He II 4541 $\text{\AA}$ . The spectra also show Balmer absorption lines within the broad emission profiles, not seen in previous spectra of CAL 87.

The difference between the out-of-eclipse and in-eclipse spectra is also shown at the bottom of Figure 1. One sees that the bluest part of the continuum and some emission lines are eclipsed during each orbit. However, in the photometry section below we will show that the apparent reddening of the continuum in the  $V$  and  $R$  bands during eclipse, reported by Alcock et al. (1997), is due to an unresolved red field star which contributes about half of the light during eclipse.

All of the individual spectra were examined as a function of time to see if the observed changes are related to the well-known orbital period ( $P=0.44$  days) or to some other time

scale. It is clear that the spectral changes are strongly phase-correlated, and we see no recognizable changes on non-orbital timescales during the 5-night run. On each individual spectrum measurements were made of the radial velocity of He II 4686Å and the line strengths of several lines. In order to measure the weakest features, the spectra were co-added in the observed wavelength frame in eight phase bins, each with a spread of no more than 0.1P in phase. The phase 0 (eclipse) and phase 0.8–0.9 bins each contain four individual spectra. The phase 0.1 bin contains two spectra, and the remaining five bins each contain three spectra. Figure 2 displays the phase-binned spectra from  $\sim 4100\text{--}4900\text{\AA}$  as well as the sum of the spectra from phases 0.2–0.8. Figure 3 shows more detail from the phase-binned spectra in region from  $\sim 4600\text{--}4900\text{\AA}$ . Using these spectra, radial velocities of He II 4686Å and several other weaker lines were measured independently by more than one author using different techniques such as parabola-fitting, line centroiding, and cross-correlating. The agreement between sets of measures was well within the estimated errors of  $\pm 5 \text{ km s}^{-1}$  in velocity and 10% in equivalent width. The mean values of all measures are listed in Table 1.

However, there are complications in making the line measurements. Some emission lines are asymmetrical and are divided by absorption components that move back and forth across them with phase (see Figure 3). The absorptions are most clearly seen at the H-Balmer lines but also may be present in He II 4686Å. It is not clear whether the He II Pickering lines are affected by absorption, but O VI, C III, and N V are probably not. In addition, the emission-line regions undergo different levels of eclipse, and this affects their profiles and hence radial velocities during the eclipse phases. In our measures we attempted to separate the absorption and emission components where possible. Emission-line velocities were based on the broad-line wings, and emission line strengths do not include the absorption components. However, where the absorption and emission velocities are close, such separation is impossible empirically. Since the absorption strength changes with phase, modeling by subtraction of a constant absorption profile is not feasible. We further discuss the consequences of these blends in a later section. Figures 4 and 5 show the phase variations of the equivalent widths and radial velocities of selected lines, respectively.

## 2.2. Photometry

To confirm the photometric ephemeris and look for possible changes in the light curve, V-band CCD photometry of CAL 87 was obtained using the CTIO 0.9-m telescope in 1994 November and 1996 November. The images were calibrated with observations of Landolt’s (1992) standard stars and reduced with DAOPHOT (Stetson 1987), in a way similar to

our earlier work. Differential magnitudes were calculated for the  $V$  filter relative to local photometric standards within the CCD frames using a procedure which minimizes errors by PSF fitting (Schmidtke 1988). A line-of-sight field star (separation  $0.9''$ , position angle  $340^\circ$ ; Cowley et al. 1991, Deutsch et al. 1996) was resolved on most images. When DAOPHOT could not separate the two stars, then the contribution of the field star was subtracted from the blended light.

The 1994 and 1996 photometry for CAL 87 is presented in Table 2. Photometric phases have been calculated using the ephemeris of Schmidtke et al. (1993), which accurately fits the new photometry and all other data we have obtained over the past eleven years. The ephemeris is:

$$T_0 = \text{HJD } 2447506.8021(\pm 0.0002) + N \times 0.4426777(\pm 0.0000016) \text{ days}$$

We note that the recent study of CAL 87 based on MACHO data obtained between 1992 and 1996 finds virtually the same period and phasing which differs from ours by only  $+0.008P$  (Alcock et al. 1997).

Figure 6 shows our  $V_{CTIO}$  photometry from all years of observation. A mean light curve, based on observations from 1985 November through 1992 December (but with most of the data from 1988–1989), is superposed. Also shown is a plot of residuals of the individual data points from this mean curve. There is a marked change in the depth of the primary minimum, particularly in the 1994 and 1996 observations which show a decrease of  $\sim 0.6$  mag in  $V$  (i.e. the eclipse became shallower). The depth of secondary eclipse also varies, but to a lesser degree. The eclipse was deepest in 1988 and shallower at all other epochs for which we have observations covering these orbital phases. The out-of-eclipse light curve does not show a corresponding brightening. The same amount of extra light which is present at primary mid-eclipse in 1996 would raise the out-of-eclipse brightness by  $\sim 0.15$  mag, but our photometry shows no change in the brightness outside of eclipse. In the bottom panel of Figure 6 the dashed line shows the effect of adding this extra source of light at all phases. While this added light fits the 1994 and 1996 CTIO data quite well through eclipse, it is clear that this amount of extra light is not present at other phases, as the majority of points lie below the dashed curve.

CAL 87 lies within one of the LMC fields monitored by the MACHO program. To further investigate the change in the depth of eclipses, we obtained public archival MACHO  $V$  and  $R$  data for CAL 87. These data have been discussed by Alcock et al. (1997) but with somewhat different objectives.  $V$  and  $R$  magnitudes had already been calculated from the broad-band red and blue colors in which the observations were made. We do not know exactly how the transformations were carried out, but we can compare the CTIO

and MACHO  $V$  light curves since we have  $V_{CTIO}$  data covering similar dates. We find that  $V_{MACHO}$  is  $\sim 0.15$  mag brighter than our  $V_{CTIO}$  data at all phases in the light curve, and we suggest that the problem may lie in the transformation of the broad-band blue color to  $V_{MACHO}$ . Unfortunately, we do not have sufficient  $R_{CTIO}$  data to compare the red light curves. Thus, for this part of the analysis we have modified our  $V_{CTIO}$  magnitudes by  $-0.15$  mag in order to intercompare directly the two data sets and study the changing eclipse depth.

Adding all of the  $(V - R)_{MACHO}$  data together, one derives a mean color of  $(V - R)_{MACHO} = -0.012 \pm 0.093$ . However, Deutsch et al. found the out-of-eclipse color of CAL 87 to be somewhat redder, with  $(V - R)_{HST} = +0.14$ . If, as suggested above,  $V_{MACHO}$  is systematically  $\sim 0.15$  mag too bright, then this would explain the bluer mean color found in the MACHO data. This also implies that  $R_{MACHO}$  is approximately similar to our  $R_{CTIO}$  values (Cowley et al. 1991).

Figure 7 shows a plot of all MACHO data obtained within  $\pm 0.03P$  of central eclipse for both  $V$  and  $R$  light. The modified  $V_{CTIO}$  minima ( $V_{CTIO} - 0.15$ ) observed between JD 2448900 and JD 2450300 are shown as crosses in Figure 7. The plot shows that the depth of minimum light has changed by almost a full magnitude during the  $\sim 4$  years of observation. The depth of primary eclipse was greatest in 1988 and least in 1995. Both  $V$  and  $R$  data, but especially  $R$ , suggest that there may be a cycle of  $\sim 600$ – $700$  days, although analysis shows this variation is probably not strictly periodic, but rather only a characteristic timescale for the changes. Similar plots have been made of the out-of-eclipse light, using data from restricted ranges of orbital phase. These show that the average light level remains unchanged through the remainder of the orbit, consistent with the analysis of “extra light” discussed above and shown in Figure 6.

One clue to understanding the change in the eclipse depth could lie in any observed color changes. Alcock et al. (1997) plot a  $(V - R)$ -color curve which appears to show that CAL 87 reddens during eclipse, but since they failed to correct their magnitudes for the effects of the red field star (discussed above) which contributes nearly half the light of the system at primary eclipse, their color curve is not correct. Using the magnitudes of Deutsch et al. (1996) which were derived from well-resolved HST images, we have corrected the  $V_{MACHO}$  and  $R_{MACHO}$  magnitudes for the presence of this nearby, unresolved star. (Deutsch et al. found yet another line-of-sight optical companion with a separation of  $0.65''$  in position angle  $210^\circ$ . However, it is much fainter than the  $0.9''$  companion and has negligible effect on the  $V$  and  $R$  light curves of CAL 87 at all phases.) In our analysis of 571 MACHO data points we have removed 24 individual points with very large errors ( $\geq 0.4$  mag) and 7 which which lie  $\geq 0.5$  mag from the light curve, since these are obviously misidentifications

or blended images (CAL 87 lies in a very crowded field). This resulted in 540 remaining  $(V - R)$  points well distributed in orbital phase. We have combined the data into 50 bins which are plotted versus phase in Figure 8. The error bars shown are the standard error of the mean. It is clear that when the correction is made for the superimposed field star there is no  $(V - R)$  color change with phase, even during eclipse. We have also examined the  $(V - R)$ -color curve for individual years and for extreme eclipse-depth values. Again, the  $(V - R)_{MACHO}$  shows no variation with orbital phase.

If there is no change in the  $(V - R)$  color through the orbital cycle, one might ask why the spectrum of the “eclipsed flux” (as shown in Figure 1) is bluer than the out-of-eclipse light. In this paper we have only  $V$  and  $R$  photometry. Since the hottest central regions of the disk are eclipsed, it may well be that a  $(U - B)$  curve would show some variation with phase, but we do not have enough  $U$  or  $B$  photometry to test this. In principle we can use our spectra to measure color changes shortward of V-band, provided we remove the field star contamination, which is small at these wavelengths. Doing so does suggest a small change in color in eclipse, but accurate photometry is required to measure it.

Considering that the depth of eclipse changes without a corresponding change in the out-of-eclipse light and that there is no  $(V - R)$  color change in the system through eclipse, the simplest explanation would be that the shape of the eclipsing body is changing. Since the companion star is unlikely to change size, this idea then implies that the eclipse is caused by an occulting region on the accretion disk rather than the secondary star (or perhaps a combination of these two). However, such a scenario seems very unlikely, given the long-term stability of the eclipse phasing. A more plausible possibility is that part of the eclipsed light comes from a hot spot on the outer part of the disk, as inferred in many cataclysmic variables. If the disk precesses, there may be periods when this hot spot is hidden during eclipse, but later becomes visible through eclipse when the angle between the disk and the observer has changed. In this picture the out-of-eclipse light would remain unchanged, as observed.

### 3. Line Strengths and Radial Velocities

In Figure 4 we see that most lines show an increased equivalent width through the eclipse, indicating that the lines are eclipsed less than the continuum and thus must arise in an extended accretion disk. The exception is O VI 5290Å, which becomes weaker near central eclipse, indicating that it is eclipsed more than the continuum and hence is formed in the innermost part of the disk.

The emission-line strengths of He II and H show an asymmetry around eclipse indicating extra flux is present in phases  $\sim 0.7$ – $0.9$  (see Figure 4). The ratio of He II 4686Å to H drops through these phases, suggesting that the extra flux is greater in the Balmer lines than in He II 4686Å (or that more He II 4686Å is hidden than H). The O VI line strength is unchanged over all phases other than during central eclipse.

The continuum is eclipsed by a factor  $\sim 4.5$ , which is approximately the equivalent-width increase of H $\alpha$  and H $\beta$ . Thus, the Balmer emission region is essentially uneclipsed and must be very large with respect to the secondary star. He II 4686Å is eclipsed to 50% of its out-of-eclipse level, and He II 5411Å is eclipsed to  $<40\%$  of its usual level. The Pickering He II lines (as shown by 5411Å) are eclipsed over a shorter phase interval, and the eclipse profile is narrower than for H and He II 4686Å. O VI is also eclipsed over a short interval to  $\sim 5\%$  of its out-of-eclipse level. These changes imply that the central hottest region, where O VI is formed, is eclipsed almost totally while the Balmer emission mostly originates in a large region which is only barely eclipsed.

Best-fit sine curves for different sets of radial-velocity data are shown in Table 3. There appear to be several different phase-related velocity variations. Velocities that represent purely orbital motion of the compact star should have maximum velocity at phase 0.75, assuming that mid-eclipse corresponds to superior conjunction of the compact star. However, the values in Table 3 clearly show that the situation is more complicated, with variable line profiles and non-orbital motions contributing to the observed velocities.

In our original paper (CSCH) we used He II 4686Å emission-line velocities to derive the stellar masses, with the orbital inclination being constrained by the light curve. The velocities showed  $K=40 \text{ km s}^{-1}$ , with phasing which showed the emission came from the region around the compact star. These velocities implied a high-mass degenerate star, much larger than a massive white dwarf. The 1996 spectra reveal that both the phasing and velocity amplitude of this line have changed, as shown Table 3. Depending on what part of the line is measured (broad base or peak) the semi-amplitude lies in the range  $\sim 26 - 33 \pm 5 \text{ km s}^{-1}$ , which implies even larger masses. However, the maximum velocity occurs at  $\phi \sim 0.6$  which is earlier than would be expected if the velocities were only due to orbital motion. If one ignores the measurements near eclipse (phases 0.9–0.1), as there could be some rotational distortion in the velocity curve due to different parts of the disk being eclipsed at different phases, the maximum velocity moves to phase  $\sim 0.65$ , but the amplitude becomes even smaller, making derived masses still higher. However, the phasing indicates there is some contribution to He II 4686Å which is non-orbital and calls into question whether we are able to determine the true orbital velocities and hence derive stellar masses from velocities of this line. We note that He II 4686Å shows a systemic



velocity of  $+273 \text{ km s}^{-1}$ , consistent with CAL 87 being a member of the LMC.

The He II  $4686\text{\AA}$  line shows asymmetries that may be partially due to superimposed weak absorption components, similar to those seen at the hydrogen lines. The H absorptions were much stronger in the 1996 spectra than in previous years. (He II  $4686\text{\AA}$  differs from the He II Pickering-series lines which do not show this asymmetry.) A blended absorption will have the greatest effect on the measured emission velocity when it is strongest and off to one side. This occurs at phases near  $\phi = 0.6$  and  $\phi = 0.1$ , so correction of the emission velocities for the presence of absorption will have the effect of increasing the velocity amplitude and causing the maximum velocity to occur later in phase.

The sine-curve fit to the ‘H $\alpha$ ’ emission velocities is shown in Figure 5 and Table 3. The amplitude is larger than for He II ( $K = 60 \text{ km s}^{-1}$ ) and the phasing later than expected from pure orbital motion. From the variation in the strength of hydrogen emissions through eclipse we have already determined that they are formed in a very large region, and hence they are probably not good indicators of the compact star’s motion. Notice that the systemic velocity for this line is  $\sim 77 \text{ km s}^{-1}$  more negative than that of He II, when the H $\alpha$  wavelength is used to compute the velocity. This is entirely consistent with the line being a blend of H $\alpha$  and He II  $6560\text{\AA}$  rather than pure hydrogen.

All of the O VI lines are too weak to be measured on individual spectra, and the  $3800\text{\AA}$  lines are very noisy. Measurements made on the phase-binned spectra of O VI  $5290\text{\AA}$  show a semi-amplitude  $K = +35 \pm 26 \text{ km s}^{-1}$ , but because the error is large this value should be taken with caution. A formal fit to velocities gives a maximum at phase  $\sim 0.83 \pm 0.11$  which, given the large uncertainty, is consistent with the expected maximum at  $\phi = 0.75$  for a line formed near the compact star. Because the  $5290\text{\AA}$  line appears to be blended with an unidentified feature on its long-wavelength side, we have not been able to determine a reliable value for its systemic velocity.

The negatively displaced  $V_0$  values of the Balmer absorption lines show that they arise in gas flowing away from the system, with the velocity component in our direction being  $\sim 80 \text{ km s}^{-1}$  more negative than the mean He II  $4686\text{\AA}$  emission velocity. Because we view the system near to the disk plane, this outflow is in all azimuthal directions, albeit with varying column density (see Figure 9). Thus, we appear to be viewing the system through a wind that has some azimuthal density and velocity variation. The absorbing medium evidently changes over timescales of years, and this change may be connected with the eclipse depth variations. An azimuthally symmetrical wind velocity would require the observed velocity change with phase to be orbital, but there may be some wind velocity change with azimuth as well, although such a wind would have to have spiral structure with respect to the disk. Because the absorption is weakest during eclipse, the absorbing gas

must be physically close to the disk. The entire Balmer absorption phenomenon appears to be different from what is seen in the supersoft X-ray binary SMC 13 (Crampton et al. 1997), where the velocity amplitude is much higher than can reasonably be due to orbital motion.

The Balmer absorptions clearly have a larger velocity amplitude than the emissions, as they move from one side to the other of the emission peaks. The absorption velocities are similar for  $H\beta$ ,  $H\gamma$ , and  $H\delta$ , showing  $K=73 \text{ km s}^{-1}$  and phasing consistent with orbital motion of the compact star. However, Figure 5 shows the velocities are very scattered, and with only six values it is very uncertain if they vary smoothly through the orbital cycle.

A very weak Ca II-K absorption line is seen in all phase-binned spectra. It may also be formed in an outflow region, as  $V_0$  is 40–70  $\text{km s}^{-1}$  lower than for He II emission. Like H absorption, this feature was not seen in spectra obtained in earlier years. The mean Ca II-K equivalent width ( $\sim 1.1\text{\AA}$ ) shows little change with phase, except for at  $\phi=0$  ( $\text{EW}=1.8\text{\AA}$ ) and  $\phi=0.5$  ( $\text{EW}=1.6\text{\AA}$ ). Thus, the Ca II absorbing column does not change much around the orbit, but it is somewhat higher near conjunctions. The maximum velocity of Ca II-K absorption occurs at an earlier phase ( $\phi=0.45$ ) than for any other lines, and its amplitude is the highest measured ( $K=97 \text{ km s}^{-1}$ ). If the velocity measured at the eclipse phase is ignored, then this result is even more extreme ( $K=155 \text{ km s}^{-1}$ ) but with the same phasing. The origin of this line is not at all clear.

Figure 9 shows a sketch of the orbit plane and summarizes the observed spectral changes. The Balmer absorption appears to be strongest in phases 0.05–0.23 and 0.6–0.7 and weakest at phase  $\sim 0.4$  and during central eclipse. The phasing of its velocity variations implies association with the accretion disk, but the changing strength of the absorption shows the column density varies with phase. Since absorption is not seen in the He II Pickering or other lines, their velocities should be more reliable than the blended H and He II emission lines for determining the motion of the compact star. However, their weakness makes them very difficult to measure reliably.

#### 4. Discussion and Summary

We have discovered that the photometric eclipse depth has changed over recent years, and this variation may even be cyclic. The increase of light observed at mid-eclipse may be due to a geometrical change in the disk structure, without a significant change in total luminosity – such as a bright structure above or below the disk plane. Alternatively, the disk may grow in size in its plane, accompanied by extra absorption due to the outflowing

material, along lines-of-sight near the center. The emergence of the Balmer absorption in the 1996 spectra suggests the latter scenario.

In 1994 November we obtained three optical spectra of CAL 87 which were reported by Hutchings et al. (1995) in their discussion of eight ultraviolet spectra observed by HST in 1995 January. We have remeasured the optical spectra, although they are of considerably lower quality than the new data and only show the strongest lines. In 1994–5 He II 4686Å and 1640Å emission-line velocities show a very different phasing (maximum velocity near  $\phi \sim 0.9$ ) and higher amplitude ( $K \sim 70 \text{ km s}^{-1}$ ) compared to both the CSCH data ( $K = 40 \text{ km s}^{-1}$ ) and present data ( $K \sim 30 \text{ km s}^{-1}$ ). The equivalent width of 4686Å was lower in the 1994 spectra than in 1996 by a factor of nearly two. In two of the three 1994 optical spectra weak absorption features are visible at H $\beta$  and H $\gamma$ , similar to those seen in 1996, but the low S/N make the velocities unreliable. Thus, it appears that there are long-term spectral changes that may include significant non-orbital motions.

The O VI lines might give a clean measure of orbital motion, as they arise in the inner disk, but they are very weak, resulting in a large velocity scatter. The measured velocity amplitude ( $K = 35 \text{ km s}^{-1}$ ) leads to the same conclusion as CSCH, that the compact star must be massive, with  $M_X > 4M_\odot$ . If instead the velocity amplitude of the compact star is shown by the Balmer absorption lines ( $K = 73 \text{ km s}^{-1}$ ), then the resulting mass diagram is almost identical to that of the supersoft binary SMC 13 (Crampton et al. 1997) and lower masses are determined. We have argued above that the measured He II velocity amplitude may be somewhat lower than the actual velocity of the compact star, because the phasing of absorptions will decrease the apparent velocity extremes, while non-orbital motions within the system add at other phases. We point out that the He II velocities in CSCH, when the eclipse was deeper, gave  $K = 40 \text{ km s}^{-1}$ . The Balmer-line velocities are also likely to contain some non-orbital motions. Thus  $K = 73 \text{ km s}^{-1}$  is a reasonable upper limit for the motion of the degenerate star. Figure 10 shows the resulting masses corresponding to these two extreme  $K$  values. The masses are constrained by the fairly well-known inclination ( $i \sim 70^\circ - 80^\circ$ ) and by the requirement that the mass-losing star fills its Roche lobe. No main sequence star fills the Roche lobe defined by these plots, for orbital inclinations larger than  $\sim 30^\circ$ . Thus, the mass-losing star must have evolved off the main sequence to cause mass-exchange. The lowest mass that can thus evolve within a Hubble time is  $\sim 0.4 M_\odot$ , and these are marked in the diagram at the appropriate inclination value. These therefore correspond to the lowest X-ray star masses under these assumptions, and just allow a white dwarf in the  $K = 73 \text{ km s}^{-1}$  case. It may be possible that the mass-losing star has very low mass by having lost most of it in some earlier event, and is still filling its Roche lobe now. However, in any of these cases the X-ray star is more massive and the resulting masses are not those expected by the ‘standard’ model (e.g. van den Heuvel et al. 1992) in which it is

assumed that the compact star is a  $\sim 1M_{\odot}$  white dwarf and the donor star has a mass of  $\sim 2.0 M_{\odot}$ .

The spectrum in eclipse shows no signs of a late type spectrum (see Figures 1, 2, 3), consistent with the absence of an evolved more massive secondary. Unfortunately, the complex changes in the disk spectrum make it difficult to be more definitive than this at present, but it appears advisable to revisit the evolutionary scenarios to accommodate a mass-losing star that is less massive than the compact star, not only in CAL 87 but also for the other supersoft X-ray binaries. We discuss separately (Cowley et al. 1998) the overall mass determinations for a number of supersoft binary systems.

Some of the supersoft X-ray binaries have been found to have highly displaced lines indicating the presence of ‘jets’. These are most noticeable in two low-inclination systems RX J0513–69 (Crampton et al. 1996) and CAL 83 (Crampton et al. 1987) where the displacements are several thousand kilometers per second. In the intermediate inclination system RX J0019+22 the jets show a velocity of  $\sim \pm 800 \text{ km s}^{-1}$  from the central emission line. The jet lines move with the same phase and velocity amplitude as the central line, suggesting that the motion of He II 4686Å emission is indeed orbital. Since CAL 87 is viewed nearly edge-on, any line emission coming from such jets would have a very low radial velocity and thus not be separated from the central emission profile. The asymmetry seen in the He II 4686Å line of CAL 87 could arise from a pair of shifted lines which have larger amplitude (or possibly slightly different phase) than the central line. This would imply that the central line motion is not entirely orbital, but without better resolution this suggestion cannot be verified.

It is a pleasure to thank the CTIO staff for their assistance during our observing runs. We also thank Dr. Douglas Welch for considerable assistance with the MACHO data. APC gratefully acknowledges NSF support for this work.

## REFERENCES

- Alcock, C. et al. 1997, *MNRAS*, 287, 699
- Callanan, P.J., Machin, G., Naylor, T., & Charles, P.A. 1989, *MNRAS*, 241, 37p
- Cowley, A.P., Schmidtke, P.C., Crampton, D., & Hutchings, J.B. 1990, *ApJ*, 350, 288 (CSCH)
- Cowley, A.P., Schmidtke, P.C., Crampton, D., Hutchings, J.B., & Bolte, M. 1991, *ApJ*, 373, 228
- Cowley, A.P., Schmidtke, P.C., Crampton, D., & Hutchings, J.B. 1998, (in preparation)
- Crampton, D., Cowley, A.P., Hutchings, J.B., Schmidtke, P.C., Thompson, I.B., & Liebert, J. 1987, *ApJ*, 321, 745
- Crampton, D., Hutchings, J.B., Cowley, A.P., & Schmidtke, P.C. 1997, *ApJ*, 489, 903
- Crampton, D., Hutchings, J.B., Cowley, A.P., Schmidtke, P.C., McGrath, T.K., O’Donoghue, D., & Harrop-Allin, M.K. 1996, *ApJ*, 456, 320
- Deutsch, E.W., Margon, B., Wachter, S., & Anderson, S.F. 1996, *ApJ*, 471, 979
- Greiner, J. 1996, in “Supersoft X-ray Sources”, ed. J. Greiner, *Lecture Notes in Physics*, 472, 299
- Hutchings, J.B., Cowley, A.P., Schmidtke, P.C., & Crampton, D. 1995, *AJ*, 110, 2394
- Landolt, A.U. 1992, *AJ*, 104, 340
- Long, K.S., Helfand, D.J., & Grabelsky, D.A. 1981, *ApJ*, 248, 925
- Pakull, M.W., Beuermann, K., van der Klis, M., & van Paradijs, J. 1988, *A&A*, 203, L27
- Schandl, S., Meyer-Hofmeister, E., & Meyer, F. 1996, *A&A*, 318, 73
- Schmidtke, P.C. 1988, *AJ*, 95, 1528
- Schmidtke, P.C., McGrath, T.K., Cowley, A.P., & Frattare, L.M. 1993, *PASP*, 105, 863
- Stetson, P.B. 1987, *PASP*, 99, 191
- Trümper, J., et al. 1991, *Nature*, 349, 579
- van den Heuvel, E.P.J., Bhattacharya, D., Nomoto, K., & Rappaport, S.A. 1992, *A&A*, 262, 97

Captions to Figures

Fig. 1.— CAL 87 summed spectra in and out of eclipse and the difference between these two spectra. The eclipse-phase spectrum is from the three observations taken between  $\phi = 0.98$  and 0.02. Notice that the Balmer absorption, seen superimposed on the emission in the upper spectrum, is not present during eclipse. Balmer emission is not significantly eclipsed. The eclipsed continuum appears to be fairly blue.

Fig. 2.— Phase-binned spectra showing the relative movement of absorption and emission Balmer components. Each spectrum is typically summed from three individual spectra within 0.1P in phase (see text). Vertical lines are at arbitrary wavelengths to enable visual alignment of features with phase.

Fig. 3.— Phase-binned spectra showing asymmetry of He II 4686Å and H $\beta$ . Spectra are spaced to allow easy viewing of the He II line peaks.

Fig. 4.— Variation of emission-line equivalent widths with phase. The peaks near  $\phi_{phot} = 0$  indicate that the emission lines are not eclipsed as deeply as the continuum. There is additional flux in phases 0.7 to 0.9 in most lines. O VI is more eclipsed than the continuum and shows no extra flux in phases 0.7 to 0.9.

Fig. 5.— Radial velocities of lines with phase. Curves in all panels show the best-fit sine curves to the points (see Table 3). *Upper panel:* Filled points are He II 4686Å emission for the whole line measured on individual spectra. The open circles represent measurements made in the phase-binned spectra. *Middle panel:* Velocities of the H $\alpha$ +HeII emission line from the eight phase-binned spectra. The relatively low mean velocity of this feature is due to use of H $\alpha$  wavelength for the blend. *Lower panel:* Velocity of hydrogen absorption measured from H $\beta$ , H $\gamma$ , and H $\delta$  in the phase-binned spectra.

Fig. 6.— The optical light curve of CAL 87. *Top panel:* A composite curve based on CTIO V data from 1985 to 1996, using the ephemeris of Schmidtke et al. (1993). The smooth curve represents the mean behavior between 1985 and 1992, but the eclipse phases are dominated by the 1988 points. *Bottom panel:* Residuals from the mean curve, showing the variable depth of primary eclipse which was noticeably shallower in 1994 and 1996. The dashed line represents the expected light-curve residuals if a constant extra-light contribution, corresponding to 0.6 mag at minimum, is added at all phases. The fact that the majority of observations lie below this line shows the extra light is not present outside of eclipse.

Fig. 7.— In-eclipse V (*upper panel*) and R (*lower panel*) magnitudes using only orbital phases  $0.97 \leq \phi \leq 0.03$  (eclipse) versus Julian Date of observation. Filled symbols are from

MACHO data; crosses are from our CTIO photometry. All data have been corrected for the  $0.9''$ -separation red field star. CTIO  $V$  magnitudes have also been adjusted by  $-0.15$  mag, since the mean out-of-eclipse  $V_{MACHO}$  data are 0.15 mag brighter than  $V_{CTIO}$  (see text for discussion of this difference). The symbol labeled ‘1988 range’ shows the range of magnitudes during phases 0.97–0.03 in the mean light curve derived from 1988 data (i.e. the blur expected in observed minima). Over the period of observation the depth of eclipse has varied by almost a full magnitude. No strict periodicity is present but the timescale of the variation is about two years.

Fig. 8.—  $(V - R)$ -color of CAL 87 versus orbital phase, based on MACHO data. The colors have been corrected for the nearby red field star, as described in the text. There is no evidence for any color change through eclipse or at any other phase in the orbit. These data include 540 individual observations taken between 1992 and 1996.

Fig. 9.— Sketch of the orbit plane illustrating the phases and lines-of-sight for the main variations measured in the 1996 spectra. The ‘abs’ refers to the Balmer absorption. Roche lobe and disk sizes are suggested, consistent with He II emission arising between the stars and O VI near the disk center. Radial velocity maxima are presumably affected by non-orbital motions and extra emission on the disk-trailing side, as expected for mass-transfer from the Roche lobe-filling companion star.

Fig. 10.— Masses of component stars for the two extreme values of velocity amplitudes discussed. The eclipse indicates an inclination of  $70 - 80^\circ$ . The dots show the implied masses for the lowest possible mass ( $\sim 0.4M_\odot$ ) of the donor star filling its Roche lobe. The mass of the accreting star rises rapidly for  $K$  values below  $40 \text{ km s}^{-1}$ . The absorption velocities are consistent with a massive white dwarf, but the emission velocities indicate a more-massive compact object. All cases require the donor star to be the less-massive component.

Table 1. CAL 87 Emission-line Measures

HJD (2400000+)	$\Phi^a$	$RV_{HeII}$ (km s <sup>-1</sup> )	Equivalent Width (Å)				
			He II 4686	H $\alpha$	H $\beta$	He II 5411	O VI 5290
50389.67	0.33	240	12	16	2.8	1.7	1.8
50389.68	0.37	291	9	18	1.1	0.9	1.9
50389.74	0.49	301	13	26	1.8	3.6	1.5
50389.75	0.53	297	12	21	1.2	1.3	2.5
50389.81	0.65	283	12	21	0.6	2.5	1.0
50389.82	0.69	315	11	23	2.1	2.2	0.8
50390.68	0.61	305	9	19	2.3	2.1	1.6
50390.69	0.64	310	9	17	1.8	1.5	1.5
50390.77	0.81	300	14	22	4.7	3.6	1.2
50390.78	0.85	304	16	23	4.5	2.1	0.9
50390.84	0.98	276	24	51	10.5	3.5	0.4
50390.86	0.02	201	21	42	9.3	2.1	0.1
50391.68	0.87	291	16	22	5.2	3.6	1.6
50391.69	0.90	272	15	24	6.0	3.1	2.5
50391.74	0.01	217	19	58	9.2	2.9	0.3
50391.75	0.04	221	15	46	5.6	2.9	0.3
50391.79	0.13	289	9	22	2.1	1.5	1.3
50391.83	0.21	253	9	14	1.1	1.8	1.4
50391.84	0.25	275	12	16	3.0	1.6	1.4
50392.66	0.09	263	12	18	2.8	1.0	1.5
50392.71	0.21	234	11	15	2.6	2.0	1.0
50392.79	0.38	289	11	15	2.0	1.7	1.2
50392.86	0.54	273	11	14	2.3	0.1	1.1
50393.81	0.69	270	11	16	2.6	1.1	1.5
50393.82	0.72	263	12	19	4.0	1.7	1.8

<sup>a</sup>See text for ephemeris.



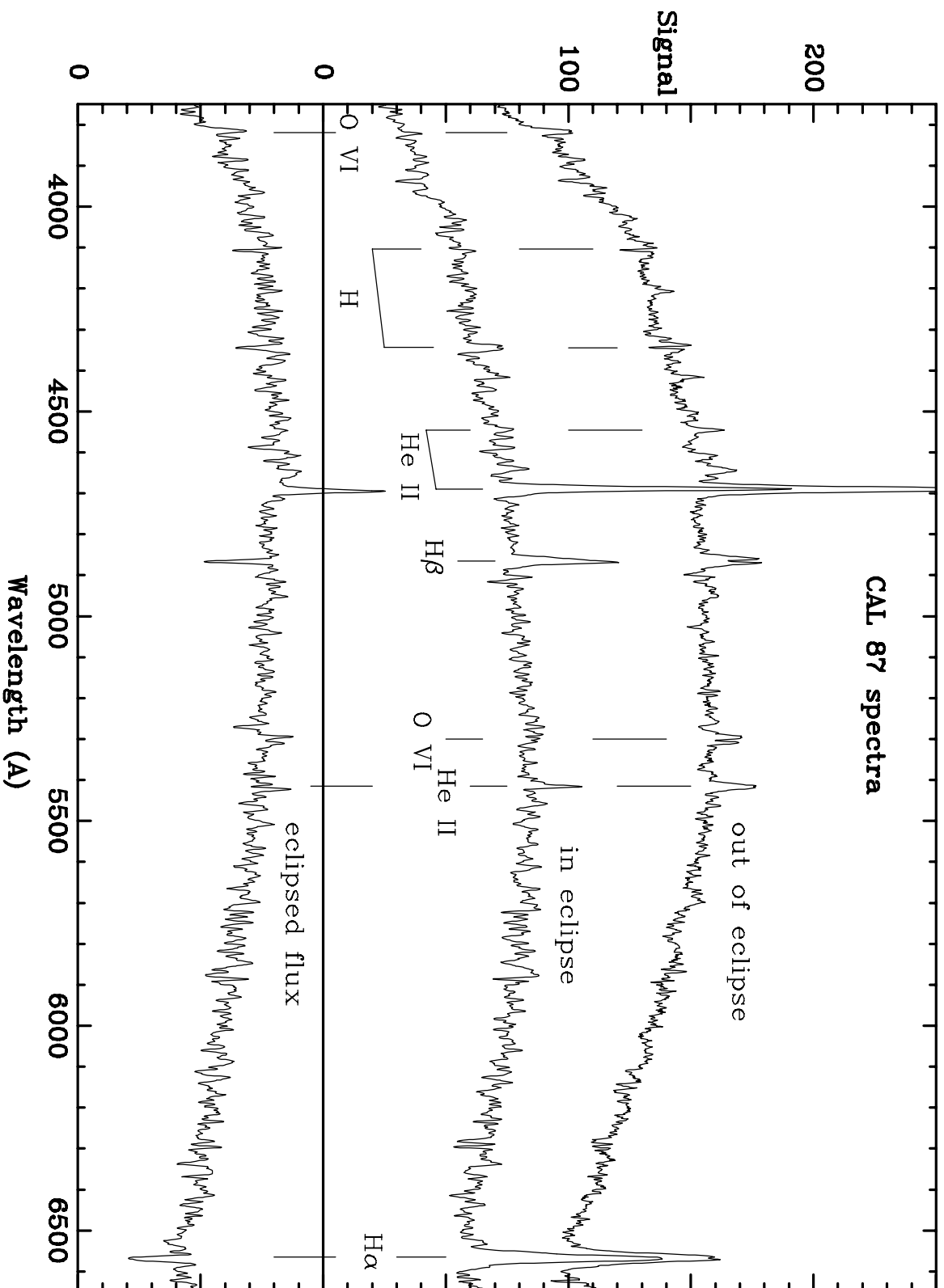
Table 2. CTIO Photometry of CAL 87 from 1994 and 1996

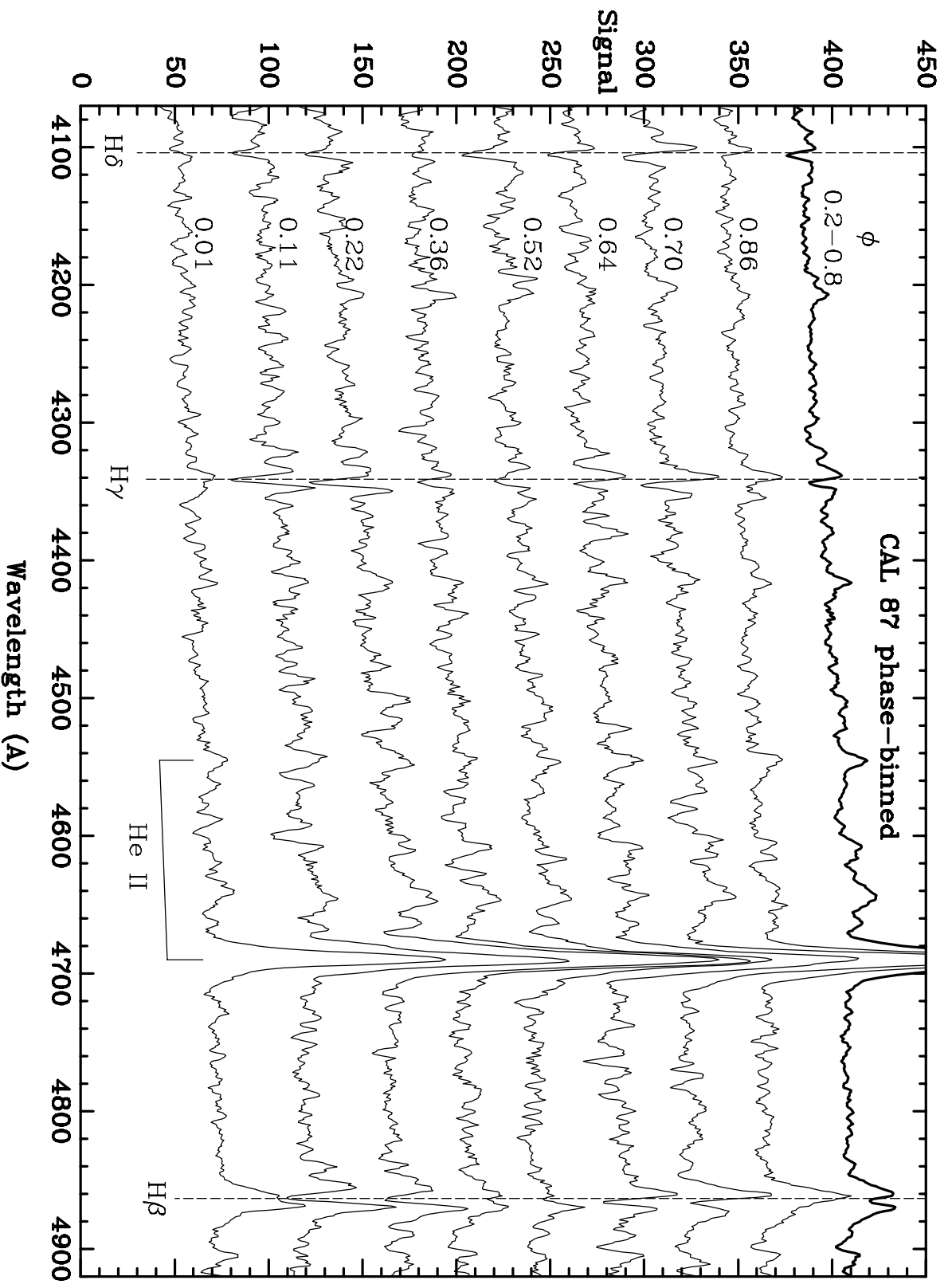
HJD (2400000+)	$V$	$\sigma_V$	$\Phi_{phot}$
49661.727	19.757	0.037	0.932
49661.743	20.095	0.030	0.967
49661.758	20.273	0.035	0.001
49661.772	19.952	0.023	0.034
49661.787	19.499	0.016	0.068
50389.799	18.894	0.025	0.631
50390.835	20.037	0.066	0.972
50391.708	19.777	0.048	0.945
50391.720	20.101	0.089	0.972
50391.732	20.197	0.076	0.998
50391.743	20.037	0.072	0.024
50391.755	19.766	0.044	0.050
50391.766	19.480	0.047	0.076
50392.719	18.893	0.031	0.228
50392.791	19.075	0.039	0.390
50393.714	19.061	0.038	0.477
50393.785	18.991	0.016	0.636
50393.854	19.310	0.022	0.792
50394.720	19.177	0.020	0.747
50394.816	19.962	0.053	0.966

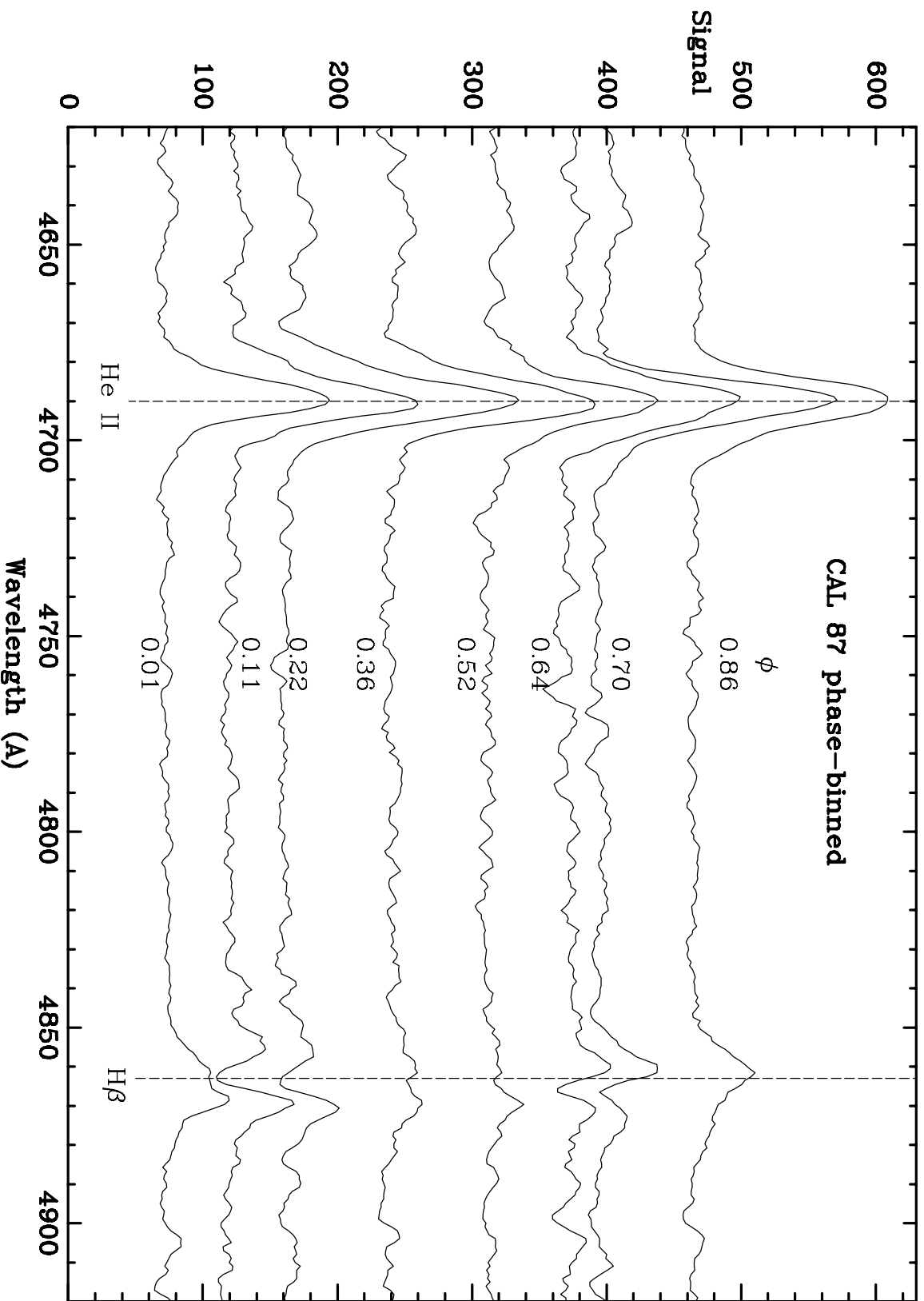
Table 3. Sinusoidal Fits to 1996 Spectroscopic Data

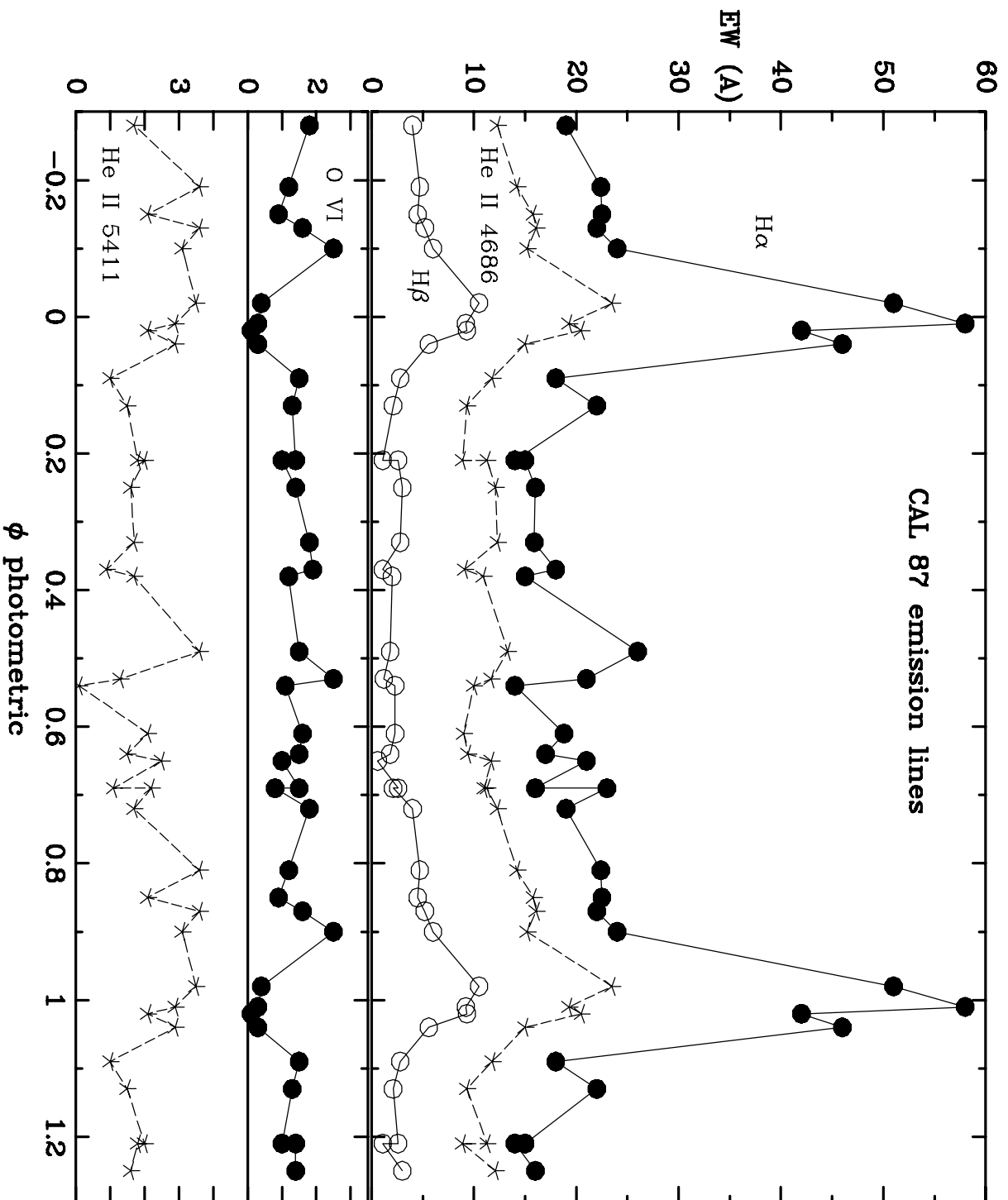
Data	$V_0$ (km s <sup>-1</sup> )	K (km s <sup>-1</sup> )	$T_0$ (phase)	Mean error <sup>a</sup> (km s <sup>-1</sup> )
He II 4686Å em – wide(all)	273±5	31±6	0.60±0.04	24
He II 4686Å em – (all)	273±5	26±7	0.61±0.04	25
He II 4686Å em – (8 bins)	273±6	33±8	0.62±0.05	18
Hα+He II em – (8 bins)	196±8	60±13	0.82±0.03	24
H abs – (6 bins)	189±44	73±47	0.72±0.17	92
O VI em – (7 bins)	- -	35±26	0.83±0.11	46
Ca II-K abs – (8 bins)	232±34	97±51	0.45±0.08	96
Ca II-K abs – (7 bins, w/o $\phi=0$ )	205±25	155±40	0.46±0.03	64
He II em (CSCH, from 1989)	306±8	40±12	0.76±0.13	

<sup>a</sup>Average deviation of observations from fitted curve.

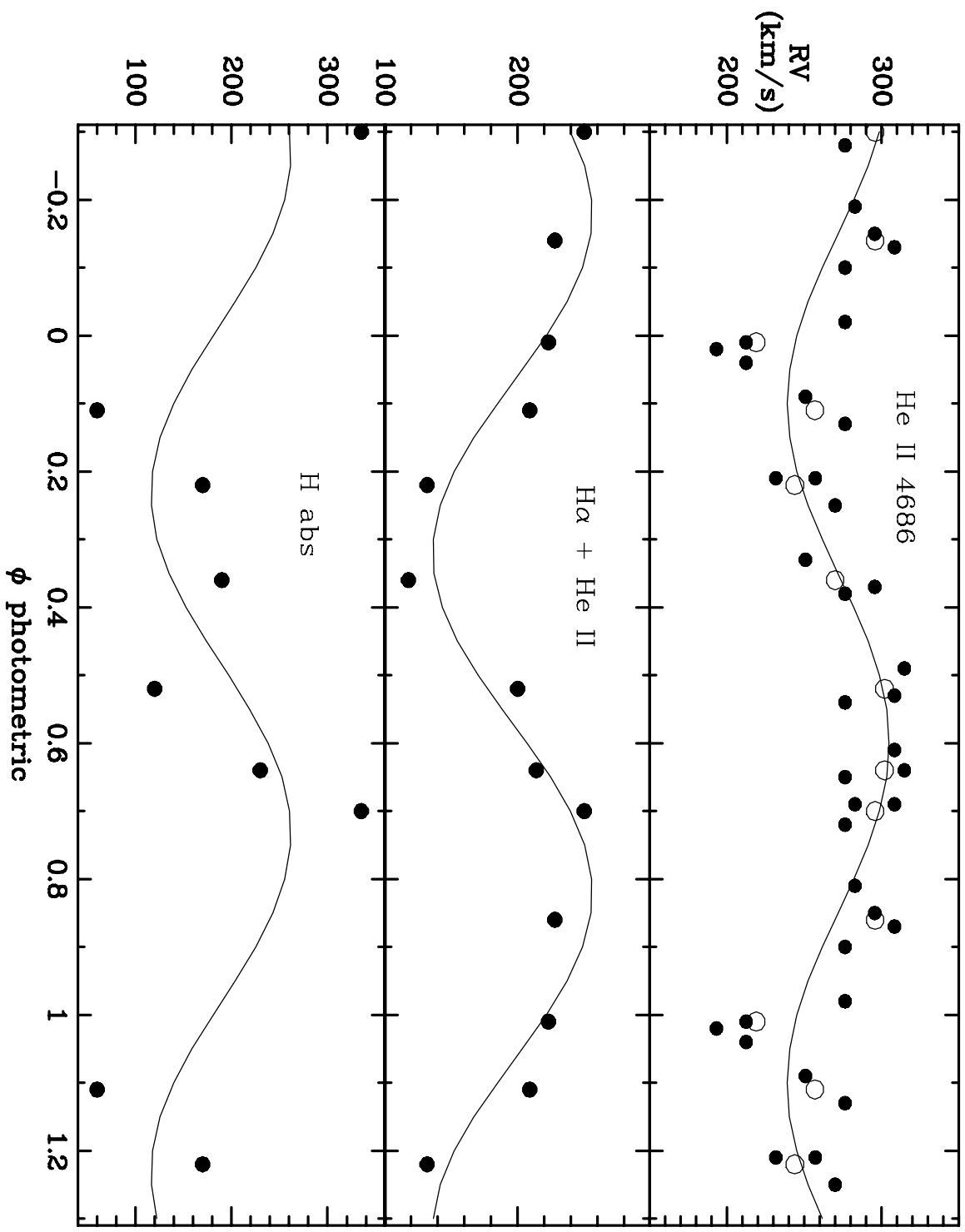


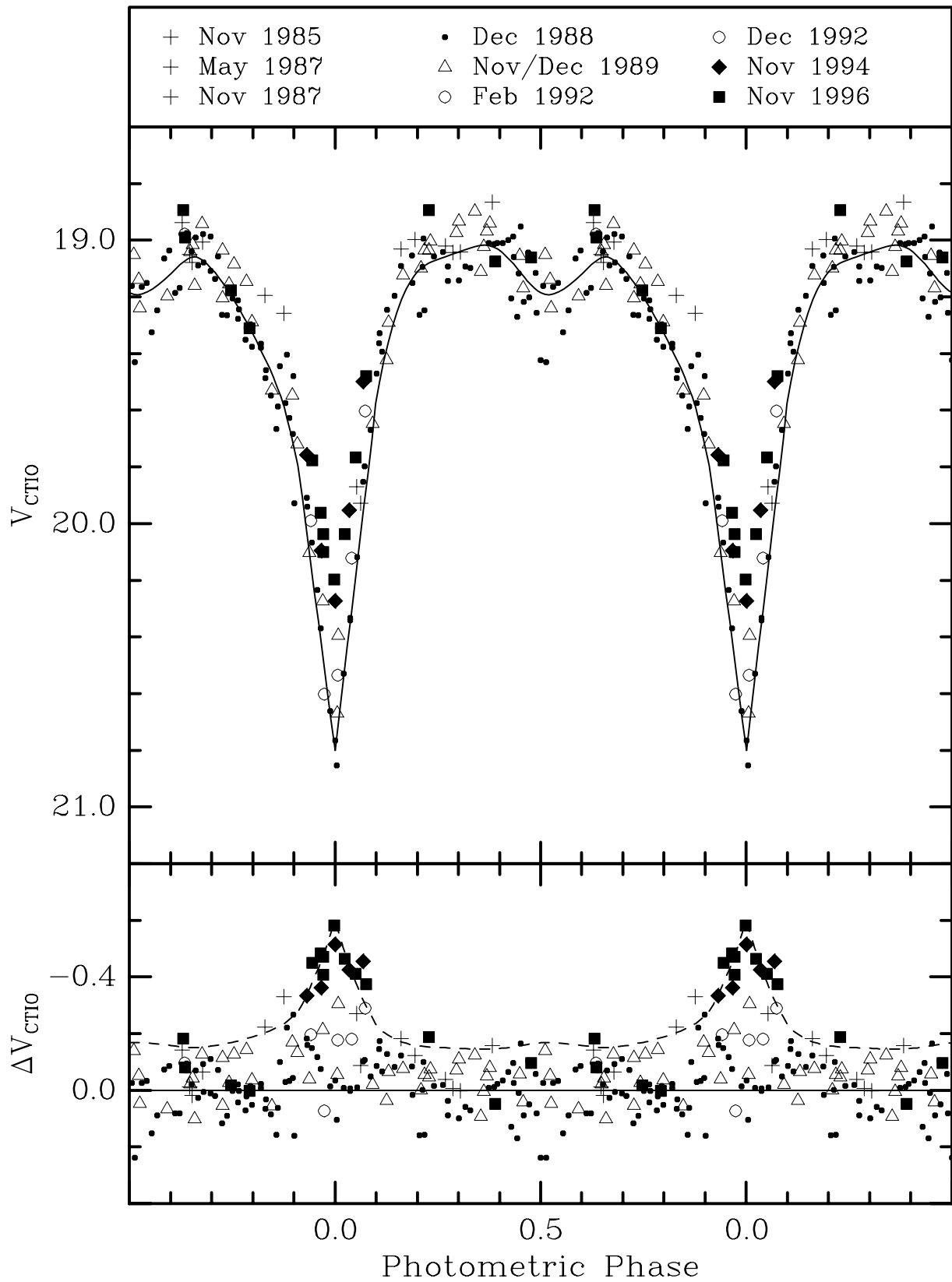




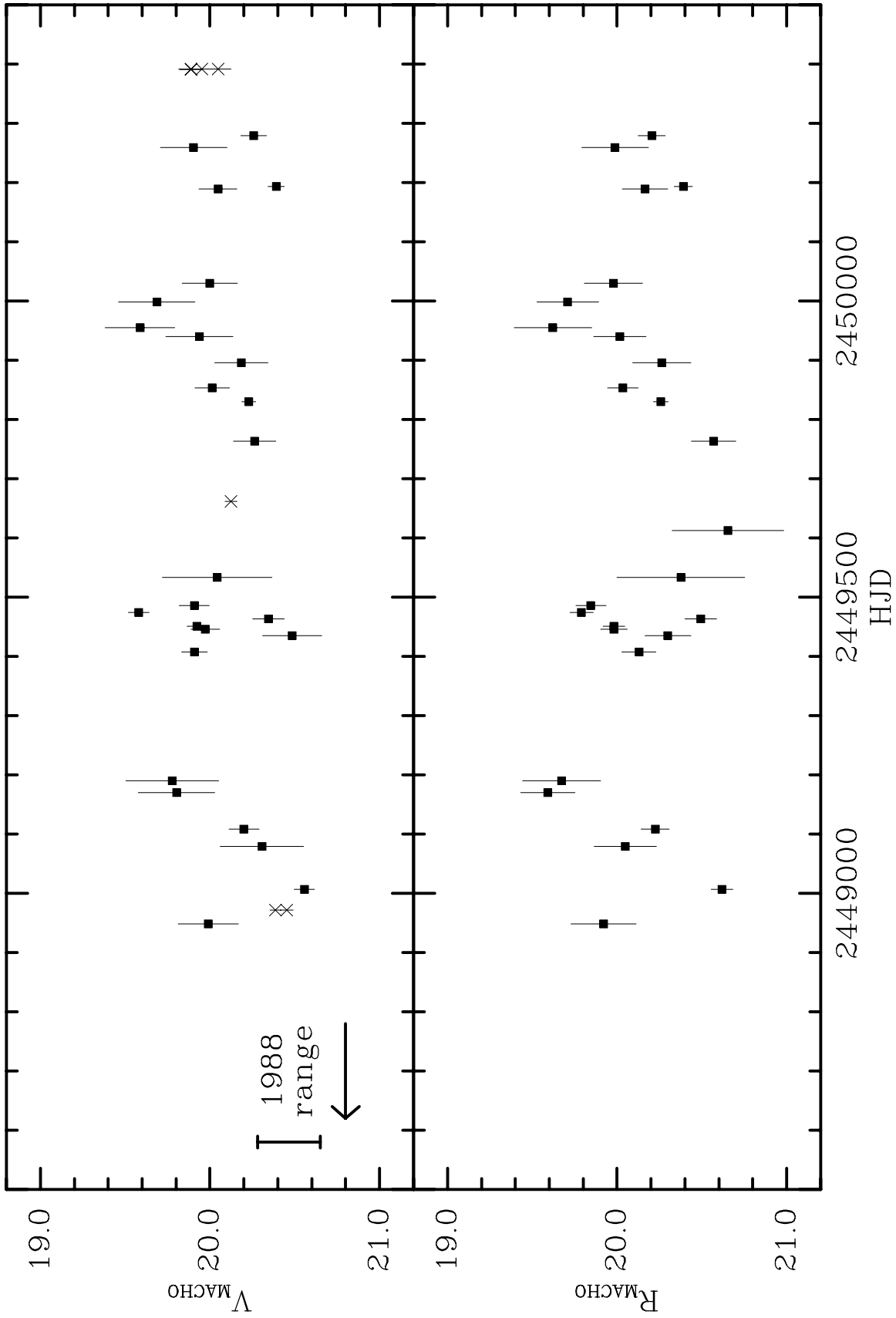


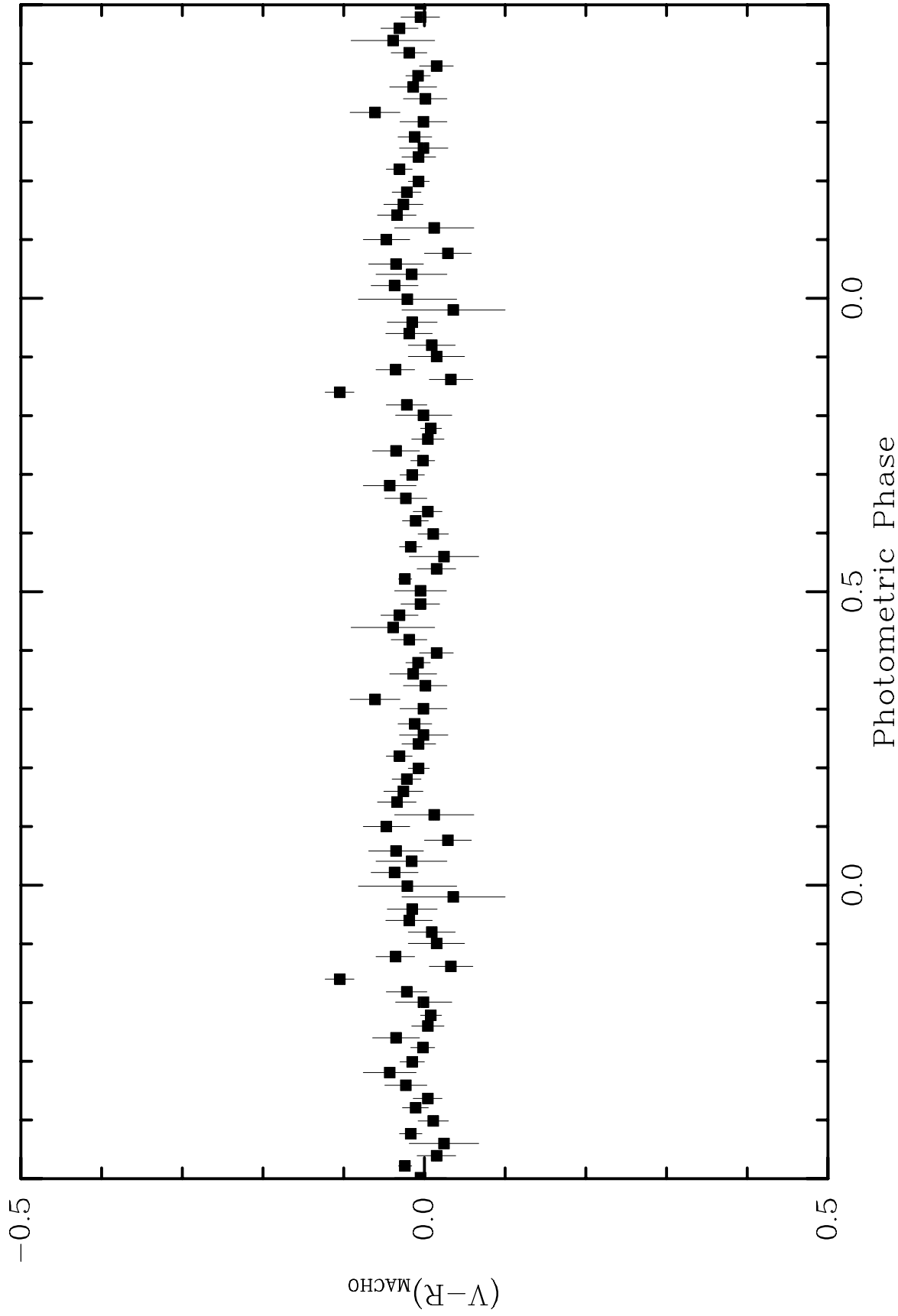
CAL 87



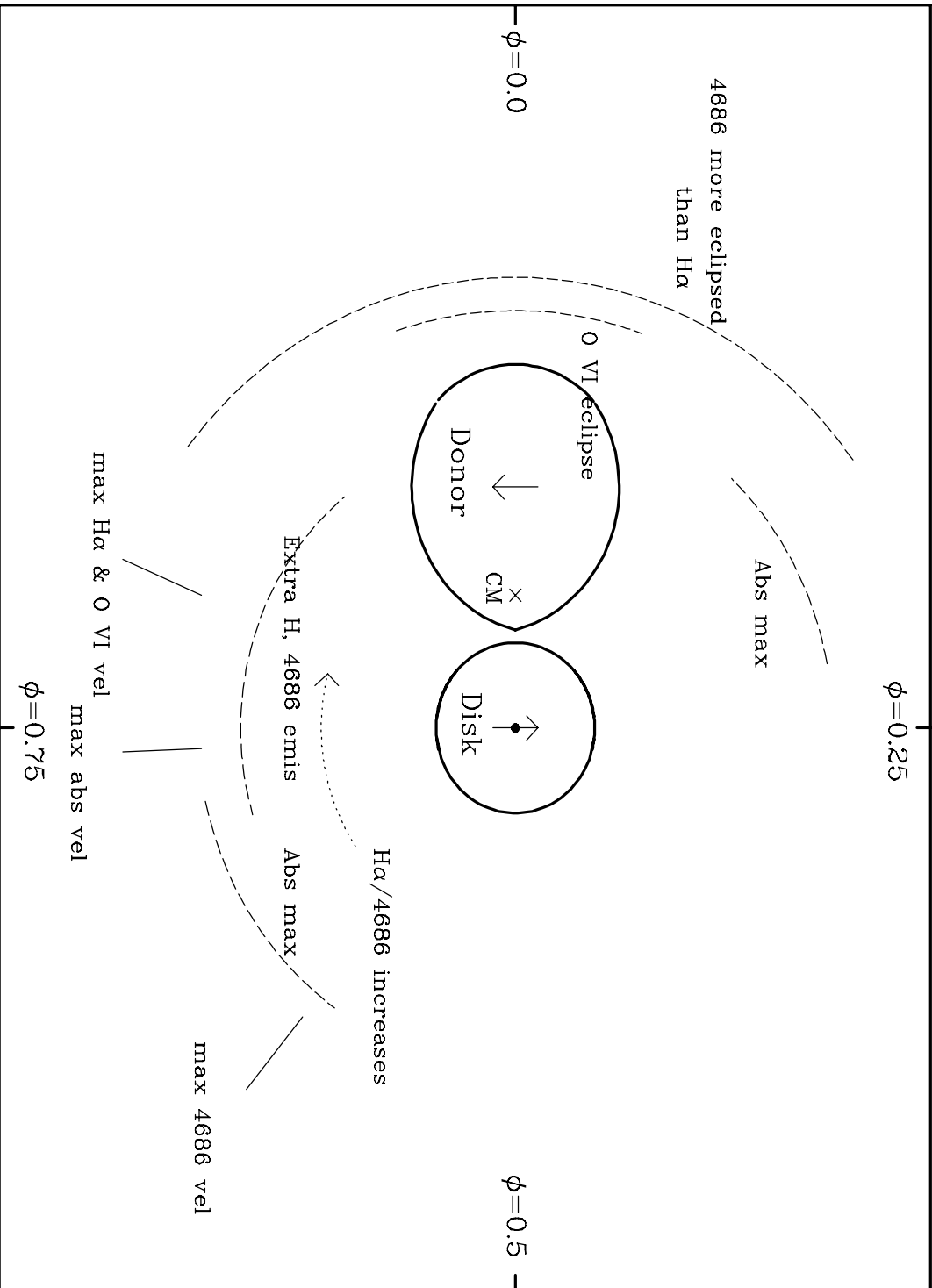








CAL 87 in 1996



CAL 87 possible masses

